Chiral symmetry breaking and chemical equilibrium in heavy-ion collisions

Sourendu Gupta[*]
Department of Theoretical Physics, Tata Institute of Fundamental Research, Homi Bhabha Road, Mumbai 400005, India

Jajati K. Nayak[†]
Variable Energy Cyclotron Centre, Kolkata 700064, India

Sushant K. Singh[‡]
Variable Energy Cyclotron Centre, Kolkata 700064, India, and Homi Bhabha National Institute, Training School Complex, Anushakti Nagar, Mumbai 400085, India

(Received 29 October 2020; accepted 16 February 2021; published 22 March 2021)

We examine the thermalization of an ensemble of the octet of pseudoscalar mesons, in the isospin symmetric limit, whose interactions are constrained through chiral symmetry, unitarity, and measurements. We use unitarized reaction amplitudes from next-to-leading-order chiral perturbation theory which generate all resonances up to masses of about 2 GeV, with 12 input parameters, namely, f_π, three masses, and eight low-energy constants of chiral perturbation theory. In linear response theory, we find that the relaxation time is around 100 fm at a temperature of 150 MeV and increases rapidly with temperature. The long relaxation times are directly related to the fact that these mesons are pseudo-Goldstone bosons of chiral symmetry breaking.

DOI: 10.1103/PhysRevD.103.054023

I. INTRODUCTION

In heavy-ion collisions, as in all collider experiments, the main observables are the particles in the final state and their momenta. Everything else of interest is constructed from these. The simplest of observables are the abundances of hadrons in the final state. In heavy-ion collisions, these yields are well explained by an ideal gas of hadronic resonances at a freeze-out temperature of $T_{\rm fo} = 158.4 \pm 1.4$ MeV [1] when the nucleon-nucleon center-of-mass collision energies, $\sqrt{s}$, is larger than 20 GeV. Furthermore, for $\sqrt{s} > 100$ GeV, the flavor chemical potentials are small. Many variants of such models have been examined [2], and they are in reasonable agreement with this result.

A coincidence arises from QCD with its approximate chiral symmetry. In the limit of exact chiral symmetry, there would have been a critical point at finite temperature and in thermodynamic equilibrium. Since the symmetry is approximate, instead there is a broad crossover [3,4] with a peak in the chiral susceptibility at $T_{\rm co} = 156.5 \pm 1.5$ MeV. This numerical coincidence has led to the identification of $T_{\rm fo}$ with $T_{\rm co}$ [1]. At present, this is the only point of contact between heavy-ion collisions and the broken chiral symmetry of hadronic physics.

Right from the early days of heavy-ion collisions there have been efforts to build a complete dynamical description of the whole history of the fireball in terms of known particle physics [5–9]. These transport computations assume that the fireball is made up of an interacting system of quarks and gluons in the very initial stages; trace their interactions; and usually find that the system approaches equilibrium, cools, and turns into an interacting system of hadrons. In this widely accepted view of the fireball, the number and momentum distribution of the final-state hadrons is a result of strong interaction dynamics. $T_{\rm fo}$ is the freeze-out temperature, i.e., the point at which the expansion rate of the fireball matches the rate of interactions, and chemistry, and eventually momenta, can no longer be kept in thermal equilibrium through interactions [7,8].

Codes which implement these approaches, like URQMD [10] and AMPT [11], incorporate a lot of known physics of strong interactions and try to predict the complete course of a collision. The hadronic interactions which are included in these approaches use many $2 \to 2$ hadron processes. A large fraction of these is not measured yet and has to

[*]sgupta@theory.tifr.res.in
[†]jajati-quark@vecc.gov.in
[‡]sushantsk@vecc.gov.in

be constrained by various model considerations. We partly follow this approach in the sense that we examine transport theory with the approximation of $2 \to 2$ interactions between hadrons. However, unlike those codes, it is not our aim to model the full course of every collision across a large range of $\sqrt{s}$.

Instead, as in Refs. [6–8], we ask a more limited question; namely, what would be the relaxation time in a hadron gas pushed slightly out of chemical equilibrium and allowed to relax back to equilibrium? The first step is to decide which hadrons should be included. Certainly, pions, which are the lightest of hadrons, need to be accounted for. It turns out that the lightest baryon, i.e., the proton, has an equilibrium number density, which is almost 2 orders of magnitude smaller at $T_{\rm fo}$. Since pion-proton and pion-pion cross sections are roughly comparable, within the accuracy of a few percent in the relaxation rates, to a first approximation, one may neglect the baryon contribution in this computation. In this first study, we will do this. Inclusion of strangeness requires us to add kaons, the lightest strange particle, to the mixture. Then, the SU(3) flavor structure would require us to add the η. So, the model contains the full octet of the light pseudoscalar mesons. These are the pseudo-Goldstone bosons of approximate chiral symmetry in QCD.

Even though it is approximate, chiral symmetry is predictive because it strongly constrains the low-energy interactions of the pseudoscalar mesons which are the pseudo-Goldstone bosons of this symmetry breaking [12–14]. Such a theory is known to be very good at predicting many properties of the lightest pseudoscalar mesons including decay constants and reaction cross sections [14–16]. In this work, we use unitarized cross sections arising from the full next-to-leading-order (NLO) computation in chiral perturbation theory (ChPT) of [16].

It turns out that they reproduce the full resonance spectrum, at least up to masses of 2 GeV. So, using the pseudoscalar octet with unitarized NLO amplitudes from ChPT seems to capture a large part of the mesonic physics that goes into the resonance gas model, while also giving enough information to make a start on transport computations. Among other pleasant aspects of the computation is that it requires a very small number of input parameters, namely, m_π, m_K, m_η, f_π, and eight low-energy constants (LECs) of NLO ChPT. After unitarization, the cross sections need no UV cutoffs. The eight LECs are obtained from other hadronic observables. We will keep track of the error bands on all of them.

Some limitations of this computation are clear enough. The neglect of baryons is a major approximation. We plan to add them in a later work. Another major limitation is that the hadronic approach is unlikely to be a reasonable way to capture the physics of the chirally symmetric state of QCD; however, that is not our concern in this work. Our main concern is to obtain a treatment of transport theory in the chiral symmetry broken region of QCD using a controllable, and independently testable, hadron theory. A step toward this is what we present here.

II. TRANSPORT THEORY IN THE HADRON PHASE

A. Chemical rate equations and relaxation times

The kinetic theory underlying chemical equilibrium and freeze-out is well known [17]. To set up our notation and the model approximations, we give a brief review here of the passage from the Boltzmann to the chemical rate equations. The Boltzmann equation for a species a in the reactive fluid can be written in the form

$$D\rho_a(x,p) = C[\rho], \tag{1}$$

where $\rho_a(x,p)$ is the Lorentz-invariant phase space density and x and p are 4-vectors for the position and momentum. We write the Liouville operator in the form $D = p_\mu \partial^\mu$, appropriate for rectilinear coordinates in flat space. The Lorentz vector number current is defined as

$$n_a^\mu(x) = \int d\Gamma_a p^\mu \rho_a(x,p), \quad \text{where } d\Gamma_a = \frac{g_a}{(2\pi)^3}\frac{d^3p}{2E}, \tag{2}$$

and g_a is the phase space multiplicity factor, which counts, in general, the dimensions of both the spin and isospin representations, i.e., $g_a = (2S_a+1)(2I_a+1)$. In our particular application, since we include only pseudoscalar mesons, $S_a = 0$. Note that the particle number density n_a is one component of this 4-vector. In the following, we will examine it in the frame in which the heat bath is at rest.

Integrating both sides of Eq. (1), one may then write

$$\partial_\mu n_a^\mu = \int d\Gamma_a C[\rho]. \tag{3}$$

The right-hand side of this chemical rate equation can be written as

$$\int d\Gamma_a C[\rho] = \int \left\{\prod_i d\Gamma_i\right\}\left\{\prod_f d\Gamma_f\right\}(2\pi)^4\delta^4\left(\sum_i p_i - \sum_f p_f\right) \times \sum_r \left[|M|^2_{r(i,f)}\left\{\prod_i \rho_i\right\}\left\{\prod_f (1\pm\rho_f)\right\} - |M|^2_{\bar{r}(f,i)}\left\{\prod_i (1\pm\rho_i)\right\}\left\{\prod_f \rho_f\right\}\right], \tag{4}$$

where the sum is over all reactions $r(i,f)$, which include the particle a among the set of initial particles i and with the appropriate set of final particles f. The reverse reaction $\bar{r}(f,i)$ interchanges the initial and final sets. Since QCD at zero chemical potentials preserves CP symmetry, one can equate $|M|_r^2$ and $|M|_{\bar{r}}^2$. Further, as long as quantum effects like Pauli blocking or Bose enhancement can be neglected, one can set $\rho \ll 1$. As a result, $1 \pm \rho \simeq 1$. Using these two approximations, one can write

$$\int d\Gamma_a C[\rho] = \int \left\{\prod_i d\Gamma_i\right\}\left\{\prod_f d\Gamma_f\right\}(2\pi)^4\delta^4\left(\sum_i p_i - \sum_f p_f\right)\sum_{r(i,f)}|M|_r^2\left[\left\{\prod_i \rho_i\right\} - \left\{\prod_f \rho_f\right\}\right]. \tag{5}$$

There are similar equations for the whole coupled chain of reactions. No assumptions need to be made at this stage about whether to use Boltzmann or quantum distributions for the distribution functions ρ. This is the form developed in Ref. [17], for example.

In the specific case that is of interest here, the temperatures could be slightly higher than the pion mass, but certainly less than twice that; $m_\pi < T < 2m_\pi$. So, reactions which produce more particles in the final state than in the initial are rare. Also, since the phase space densities are much less than unity, collisions of three or more particles are extremely rare. As a result, one can restrict a first investigation to reactions involving two particles in the initial state and two in the final state, i.e., $2 \to 2$ reactions. In this case, further reduction of eq. (5) is possible.

The total cross section for the forward reaction $ab \to cd$ is

$$F_{ab}\sigma_r = \int d\Gamma_c d\Gamma_d (2\pi)^4\delta^4(p_a + p_b - p_c - p_d)|M|_r^2, \tag{6}$$

where the Lorentz-invariant definition of the flux of particles in the initial state is $F_{ab}^2 = (s - (m_a + m_b)^2)\times(s - (m_a - m_b)^2)$, where s is the square of the c.m. energy in the collision of a and b [18]. One can use a similar expression for the cross section, $\sigma_{\bar{r}}$, of the reverse reaction, $cd \to ab$. One may trade the squared matrix element on the right for the combination on the left in the rate equation, if one wants to.

We will now choose to work in the frame in which the heat bath is at rest. Our model consists of the fluid at rest in this frame so that the spatial components of n_a^μ vanish, and the time component is the particle density. Then, the rate equation becomes

$$\frac{dn_a}{dt} = -\sum_r \langle\langle \sigma_r v_{ab}\rangle\rangle n_a n_b + \sum_{\bar{r}} \langle\langle \sigma_{\bar{r}} v_{cd}\rangle\rangle n_c n_d. \tag{7}$$

Here, we have used the notation $v_{ab} = F_{ab}/(4E_aE_b)$; a Lorentz covariant definition of v_{ab} follows from the above definitions. Further, the double angular bracket indicates averaging over the instantaneous densities of the initial particles for a reaction. However, these nonequilibrium distributions are not universal, and a general study is not of much interest. It is more useful to examine this in the linear-response limit as the system reaches close to equilibrium.

Accordingly, we set $n_a = n_a^{\rm eq} + \delta n_a$; expand in the small deviations from equilibrium, δn_a, etc.; and retain terms up to linear order in these small parameters. The terms independent of the δns vanish due to detailed balance. We can then replace averages with respect to the nonequilibrium distributions by averages in equilibrium. These are denoted by single angular brackets below. To linear order, the reaction rate equations become

$$\frac{d\delta n_a}{dt} = -\sum_r \langle\sigma_r v_{ab}\rangle(n_b^{\rm eq}\delta n_a + n_a^{\rm eq}\delta n_b) + \sum_{\bar{r}} \langle\sigma_{\bar{r}} v_{cd}\rangle(n_d^{\rm eq}\delta n_c + n_c^{\rm eq}\delta n_d). \tag{8}$$

The linear system of equations can be represented in the form $\dot{\mathbf{n}} = -A\mathbf{n}$, where $\mathbf{n}$ is a column vector whose elements are each of the deviations of the number densities of interest from their equilibrium values. Each element of the matrix A is a quantity of the form $\langle\sigma v\rangle n$. One sees that dimensionally this is the inverse of a time (we have used natural units throughout). For every conserved quantity, one has a zero eigenvalue of A. Every other eigenvalue of A is the inverse of one of the relaxation times of the system.

The longest relaxation time tells us how fast the disturbed system relaxes back to chemical equilibrium. Far away from equilibrium, the system can relax either faster or slower. However, as the system approaches equilibrium, the rate of approach to thermal equilibrium cannot be faster than the inverse of the longest relaxation time [8]. We relate these relaxation times to freeze-out in the next subsection.

B. Expansion timescale and freeze-out

If chemical freeze-out occurs somewhat late in the lifetime of the fireball, then one may approximate the fluid flow by a uniform radial flow. It is most convenient in this case to choose radial coordinates in the c.m. frame of the fireball. We can then write the Liouville operator in these curvilinear coordinates and find that the linearized form of the chemical rate equations become

$$\frac{d\mathbf{n}}{dt} + \frac{3}{t}\mathbf{n} = -A\mathbf{n}, \tag{9}$$

where the components of $\mathbf{n}$ are the deviations from the equilibrium value of each of the densities, A is the same matrix as before, and t is the elapsed time in the chosen frame. A small formal remark is in order: the square matrix A is not symmetric. Since the vector n is defined to be a column vector, and A acts on it from the left, the right eigenvectors are the ones which specify the normal modes of the system. The eigenvectors need not be orthogonal to each other. This equation now allows a simple dimensional argument for the freeze-out time (see also Refs. [7,8]).

Each eigenvalue of A, λ_i, is the inverse of the relaxation time, $\tau_i = 1/\lambda_i$, of one of the eigenmodes of the fluid when

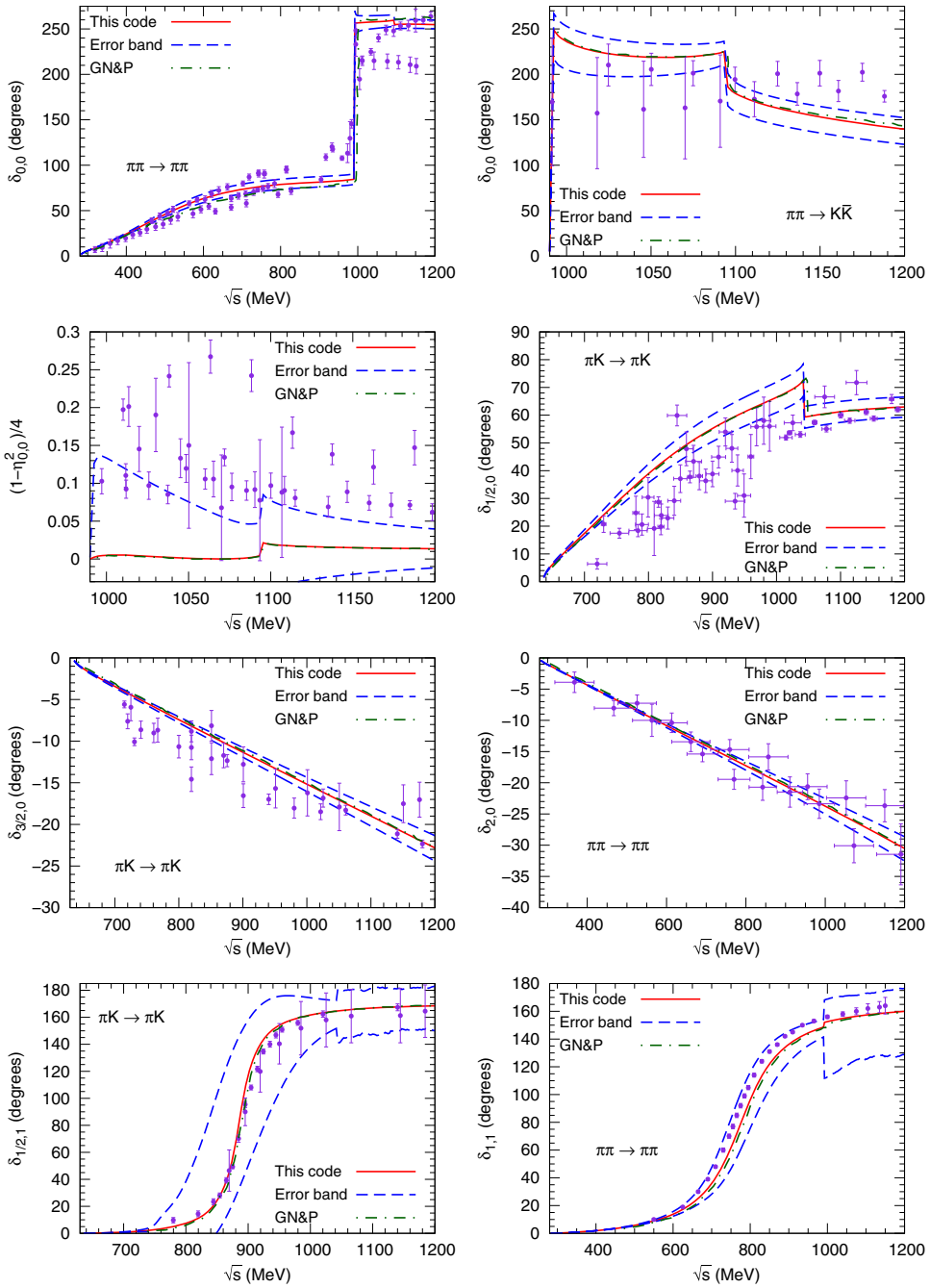

FIG. 1. Scattering phase shifts, $\delta_{I,J}$, and inelasticity, $\eta_{I,J}$, in the scattering of pions and kaons for isospin, I, and angular momentum, J, channels, shown as a function of the c.m. energy of the colliding mesons ($\sqrt{s}$). The dot-dashed lines (labeled GN&P) shows the results reported in Ref. [16], the full line shows the central values of our results, and the dashed lines denote the error bands on the predictions obtained by sampling the error bands of individual LECs through a Gaussian distribution.

there is no flow. Every conservation law gives an exact zero eigenvalue; these may be disregarded for the analysis of freeze-out. If the other $\tau_i \ll t/3$, then any deviation from equilibrium dies away much faster than the expansion rate, and the fluid may be considered to be in chemical equilibrium as it expands. If one of the $\tau_i > t/3$, then the corresponding eigenmode of A will not be able to relax back to equilibrium, and that mode may be considered to have frozen out. The subsequent evolution of the fluid involves the frozen mode(s) as well as modes which may remain in equilibrium. If there is a big hierarchy between the chemical relaxation times, τ_i, then it may be possible to use sequential freeze-out scenarios, which are common in cosmology [17] and have been proposed in heavy-ion collisions [2].

We note that at very large times, t, the formal solution of the above equation may still allow $\tau_i \ll t$. However, the system will have diluted to the point that a hydrodynamic flow is no longer feasible. Even if the τ_i are so small that radial flow is not a very good approximation at $t \approx \tau_i$, a dimensional argument shows that hydrodynamic expansion of the fireball would change the factor $3/t$ to ξ/t where the dimensionless number ξ depends on the details of the flow. With this change, the arguments given above would continue to be applicable.

C. Hadron cross sections from chiral perturbation theory

As discussed earlier, in this paper, we report an investigation of a model hadron fluid made of the pseudo-Goldstone bosons of chiral symmetry breaking, namely, the lowest SU(3) flavor octet of pseudoscalar bosons. The mutual interactions of these mesons are completely constrained by chiral symmetry [13–15], and their reaction cross sections have been computed in ChPT. We use the full set of unitarized amplitudes which were presented in Ref. [16]. These include the amplitudes for the reactions $\pi\pi \leftrightarrow \pi\pi$, $K\bar{K} \leftrightarrow K\bar{K}$, $\pi\pi \leftrightarrow \eta\eta$, $\pi\pi \leftrightarrow K\bar{K}$, $\pi\pi \leftrightarrow \eta\eta$, $K\bar{K} \leftrightarrow \pi\eta$, and $K\bar{K} \leftrightarrow \eta\eta$, with all the allowed crossings. The amplitudes depend on the meson masses, f_π, and eight other LECs ($L_1, L_2 \cdots, L_8$) which appear in the Lagrangian of ChPT to order p^4.

Discussions of the extraction of the LECs from hadron observables can be found in Refs. [14,15]. L_1, L_2, and L_3 can be determined through $\pi\pi$ scattering in the $J = 2$ channel and from the weak decays of K. Constraints on L_1, L_3, L_4, and L_6 come from Zweig's rule. L_5 may be determined by the f_π to f_K ratio. L_4 and L_6 are also obtained from the π scalar and charge radii. L_5, L_7, and L_8 are constrained by the Gell-Mann-Okubo mass formulas. We have used the values from Ref. [16]. Currently, error bands in individual constants range from 25%–40%. In this work, we shall exhibit the uncertainties in predictions due to the current range of uncertainties in these constants.

Two implementations of unitarized amplitudes from ChPT are discussed in Ref. [16]. In one, the dimension of the T-matrix is taken to be equal to the number of channels which are open so that the dimension changes at every mass threshold. This strictly implements unitarity at each energy but may result in a discontinuity of the amplitude at thresholds where new channels open up. The other is to use a constant dimension for the T-matrix, equal to the highest dimension required until about 2 GeV. This may result in a loss of unitarity in the vicinity of a threshold, but preserved continuity. The difference between the two methods for phase shifts was shown to be minor. In our implementation, we chose the first approach so that unitarity is always strictly implemented.

In Fig. 1, we compare our numerical implementation with that of Ref. [16]. In the figures, we have also given the theory errors on the phase shifts induced by the errors in the input LECs. These are estimated by Gaussian sampling of the range of allowed variation for each of the LECs separately. See the Appendix A for further discussion of this theory uncertainty. We note that keeping track of theory errors is important, as one sees in Fig. 1.

The phase shifts δ_{11} and $\delta_{1/2,1}$ show very clearly the presence of the ρ and K^* mesons. A closer investigation shows that the interacting gas of pseudoscalar mesons generates the full SU(3) octet of vector mesons. We also checked that the interacting system generates all scalar mesons with masses less than 2 GeV. There are no tensor mesons in this mass range, so the interacting system of SU(3) octet of pseudoscalars generates the hadron resonance gas of all SU(3) octets with masses less than 2 GeV. We use these amplitudes to compute the elements of the matrix A defined after Eq. (9).

We note that earlier work along these lines [6,7] also used ChPT. However, they predated Ref. [16], as a result of which the resonance region was then not captured by this fundamental approach. So, parametrizations were used to describe amplitudes in the resonance region. We are able to avoid this due to advances in QCD, which allows us to proceed with a small number of LECs in ChPT, which may be determined by measurements of other hadron properties, and to write unitary amplitudes for the transport theory without any *ad hoc* UV cutoff.

III. RESULTS

In this paper, we neglect the differences in masses due to SU(2) isospin breaking and treat all pions as having a mass equal to the mean mass of the isotriplet. We also take all the kaons to have exactly equal mass and that of the mean mass of each isodoublet. The matrix elements then distinguish four classes of mesons: pions, whose number density we denote by n_π, kaons (with strangeness of -1) having number density n_K; antikaons (strangeness of $+1$) with number density $n_{\bar{K}}$; and η with number density n_η. The linearized reaction matrix A is then a 4×4 matrix.

Collapsing each isospin multiplet into one species means that we cannot examine thermalization times associated with isospin fluctuations. This is an interesting issue which could be addressed by a fundamental approach such as the one we take. However, the main interest in this question is due to isospin fluctuations in the baryon sector, so we defer this question for later.

The computation of the reaction rate matrix A requires $n^{\rm eq}(m,T)$. We use the expansion of the number density from the Bose distribution

$$n^{\rm eq}(m,T) = \frac{gm^2T}{2\pi^2}\sum_{j=1}^{\infty}\frac{1}{j}K_2\left(j\frac{m}{T}\right), \tag{10}$$

where K_2 is the modified Bessel function of order 2, which decays exponentially as a function of its argument. For temperatures in the range up to 160 MeV or so, ten terms of the series are sufficient to get the number density accurate to five places of decimals for the pion. For the remaining mesons, the leading term suffices. This corresponds to the classical Boltzmann gas approximation.

The unitarized amplitudes require a partial wave expansion of the expressions obtained from ChPT, and, up to the order at which the amplitudes are available, it is sufficient to keep terms only up to $J = 2$. It is most convenient to do this expansion numerically. Our codes used standard LINPACK routines for unitarization and inversion of matrices and QUADPACK routines for integrals. Since our matrices are extremely small (3×3 at most), we also experimented with simpler high accuracy inline code for eigenvalues and inverses; these improved run times slightly without compromising accuracy. For the hadronic matrix elements, we found unitarity of the S-matrix in all channels up to machine precision for center-of-mass energies of a little over 2 GeV. Computations of $\langle\sigma v\rangle$ used Gauss-Laguerre routines for the integration over momenta and Gauss-Legendre routines for angular integrations. We checked that numerical rounding and truncation errors lie well below the theoretical uncertainties due to the input hadron parameters. The comparisons shown in Fig. 1 are part of the check of our codes.

There are two conserved quantities: net strangeness and total particle number (since we used only $2 \to 2$ reactions: see Appendix B). As a result, there are two eigenvalues of A which vanish. It is simple to actually parametrize the number densities so that this is taken account of. We can write $n_\pi = n_\pi^{\rm eq} + h_\pi$ and $n_\eta = n_\eta^{\rm eq} + h_\eta$. Then, one has $n_K = n_K^{\rm eq} - (h_\pi + h_\eta)/2$ and $n_{\bar K} = n_{\bar K}^{\rm eq} - (h_\pi + h_\eta)/2$. Substituting these parametrizations in Eq. (9), one can eliminate two of the equations to obtain the reduced set of equations

$$\frac{d\mathbf{h}}{dt} + \frac{3}{t}\mathbf{h} = -C\mathbf{h}, \tag{11}$$

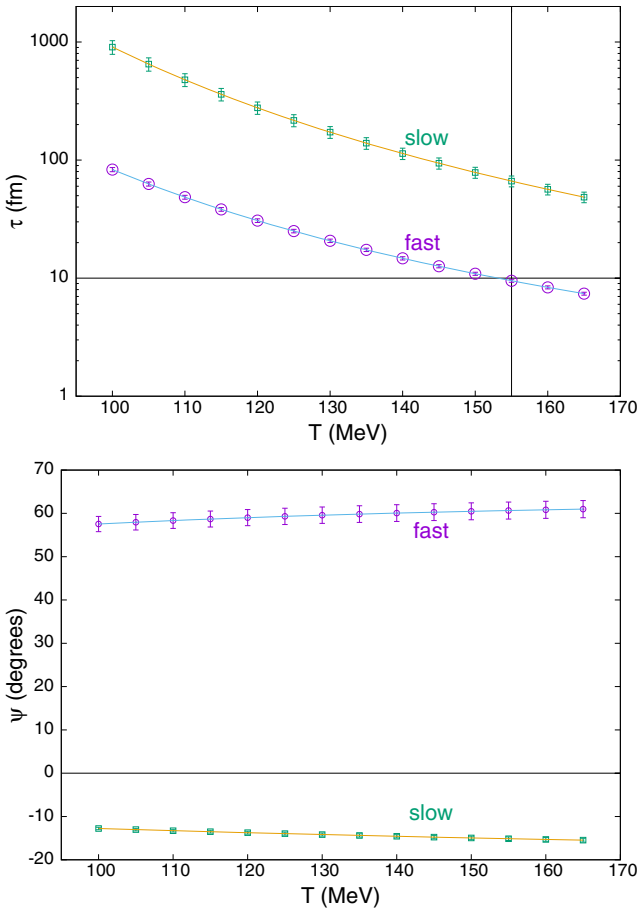

FIG. 2. The relaxation times, τ, for the two normal modes of the linearized chemical rate equations are shown in the first figure as a function of the temperature. The eigenmodes are shown in the second figure; ψ is the angle the eigenvector makes with the pion direction. In both cases, the error bands shown are obtained from a Monte Carlo sampling of parameters, as described earlier.

where $\mathbf{h}$ is a two-dimensional column vector whose components are h_π and h_η, respectively, and C is a reduced matrix obtained from A by eliminating the equations for n_K and $n_{\bar K}$ using the conservation laws. The eigenvalues of C are the inverses of the relaxation times of the system. The two eigenvectors can be specified by the angle, ψ, that they make with the h_π axes.

The results of our computations are shown in Fig. 2. At a temperature of about 150 MeV, the fast mode has a relaxation time of around 10 fm. This increases to about a 100 fm at a temperature of 100 MeV. The slow mode is an order of magnitude slower, with a relaxation time of around 100 fm at $T = 150$ MeV, growing to around 1000 fm at $T = 100$ MeV. We note that this growth by a factor of about 10 is slower than the factor of about 100 seen over the same range when leading-order ChPT was used in Ref. [6]. The slow mode is dominantly of pions relaxing toward equilibrium; the eigenvector makes an angle of 10 to 15 degrees with the pion direction. The fast mode is

dominated by the relaxation of the η, since it makes an angle of about 30 degrees with the η direction.

The interactions of Goldstone bosons are strongly constrained and involve derivative interactions, which are forced by symmetry. The fact that quark masses are nonzero allows nonderivative couplings. A signal of this is that the mode dominated by the highest mass pseudo-Goldstone boson, the η, has lower relaxation time. We can check this also by dropping the η meson from the computation. Removing it should decrease the net cross sections and push up the relaxation time. After removing the two conservation laws using the equations for n_K and $n_{\bar{K}}$, and writing the equation for the pion in terms of h_π, its deviation from equilibrium, one can write the linearized chemical rate equation as

$$\frac{dh_\pi}{dt} + \frac{3}{t} h_\pi = -\frac{1}{\tau'} h_\pi, \tag{12}$$

where the relaxation time, τ', of the gas without the η is computed using the remaining amplitudes. The result is about an order of magnitude larger than τ_s. The movement is in the direction that we expected from the argument based on ChPT. In Ref. [6], a similar order of magnitude change was found when comparing a pure pion gas with the more complex hadron gas, which was used there.

Relaxation times of 100 fm may seem unnatural in a hadron gas, where typical timescales are expected to be around 1 fm. However, one may recall that $1/\tau \simeq \sigma n^{\rm eq}(m_\pi, T)$, where σ is an average over the hadron cross sections and $n^{\rm eq}(m_\pi, T)$ is given by eq. (10). The fact that the eigenvector corresponding to the slow mode is almost fully aligned with the pion direction shows that this assumption is fairly accurate. In a theory of pions, one would expect $\sigma \simeq m_\pi^2/(4f_\pi^4)$. It turns out to be useful to use the dimensionless ratio

$$\Pi_s = \tau_s(T) n^{\rm eq}(m_\pi, T) \left(\frac{m_\pi^2}{4f_\pi^4}\right), \tag{13}$$

where τ_s is the relaxation time of the slow mode. With the values of τ_s shown in Fig. 2, we find that Π_s is unity at $T = 100$ MeV and varies only by a factor of 2 over the full range of temperature shown. This provides a check that the very long relaxation time is natural and that its magnitude is what should be expected. A dimensional argument is not sensitive to constant factors, so one may consider that the factor 4 in eq. (13) is used to make $\Pi_s \simeq 1$ at $T = 100$ MeV or to match the low-energy total $\pi\pi$ cross section to its physical value of about 25 mb [19]. The surprise is that the two statements are equivalent; i.e., a simple kinetic theory argument for τ_s is nearly right. This seemingly simple result arises only when NLO ChPT with unitarization reproducing the meson resonances is used. The leading-order results of Ref. [6] or the lack of an incomplete octet of Goldstones spoils it. The slow increase in Π_s with T is also a sign of the complexity of the dynamics captured in the higher-order ChPT that we used.

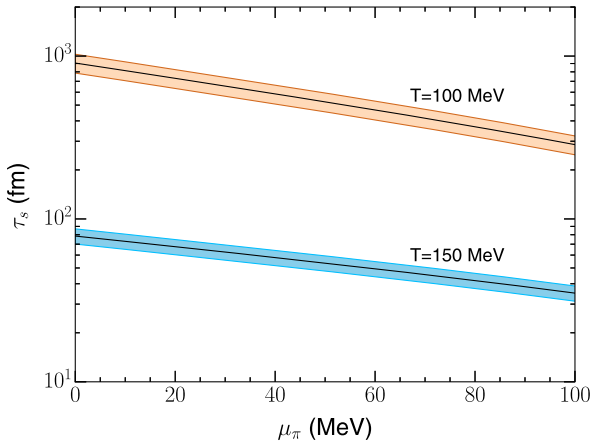

FIG. 3. The relaxation time of the slow mode, τ_s, shown for a range of μ_π, computed using eq. (13). The error band comes from the statistical errors shown in Fig. 2. The hadron resonance gas description of heavy-ion collisions usually corresponds to $\mu_\pi \approx 0$, although values as large at $\mu_\pi \simeq 70$ MeV have been used on occasion.

A further test of the chiral symmetry operating behind these observations comes by examining the relaxation time of the fast mode, τ_f. For this, one can compute the dimensionless ratio $\Pi_f = \tau_f(T) n^{\rm eq}(m_\eta, T) m_\eta^2/(4f_\eta^4)$. Again, this turns out to be of order unity, varying from about $2/3$ to $4/3$ over the same range of temperature. The use of the quantities for η in this case is suggested by the large component of the fast eigenmode in the η direction. Both the fast and slow modes turn out to be natural. The unexpected size of the relaxation times is due essentially to the fact that the equilibrium densities of the mesons at these temperatures are small.

If the early dynamics of the fireball somehow produces an overabundance of particles in some parts of phase space, then this can persist into the hadronic phase, which is dominated by $2 \to 2$ collisions, which cannot change the total number of particles. Then, one might have a situation in which a description of the meson gas requires a chemical potential for each species (see Appendix B). The relaxation times in such a gas are expected to be smaller because of the decreased mean free paths. A quantitative description of such a situation is provided by eq. (13) and is shown in Fig. 3. We see that the relaxation times can drop to as low as 30–40 fm when the chemical potential is as high as 100 MeV.

IV. CONCLUSIONS

We examined the chemical relaxation time in a gas of the SU(3) octet of pseudoscalar mesons in the linear response approximation. The reaction amplitudes in the gas were described by the best current results in ChPT available to date [16]. These interactions generated the full SU(3) octet

of vector mesons and all the scalars up to 2 GeV in mass. The dynamical generation of resonances is one of the most useful aspects of these cross sections and allows us to proceed without further free parameters. The amplitudes are completely parametrized by three masses, one decay constant, and eight LECs of ChPT, all of which are known from experimental observables. No ultraviolet cutoff was needed because we used unitarized amplitudes.

We made a careful analysis of the theoretical uncertainties which arise from uncertainty in the values of the LECs. These are included in all our results. Another source of uncertainty is the lack of knowledge of higher-order terms in ChPT. Their effects are subdominant except in the vicinity of resonances with higher angular momenta. It was argued in Ref. [6] that such higher resonances have a minor effect on relaxation times.

We found that the slowest relaxation time, τ_s, which controls the rate of approach to equilibrium, is about 100 fm, just below the QCD crossover temperature. We found that its magnitude was natural, and essentially captured in the formula $1/\tau_s \simeq n_\pi^{\rm eq}\sigma$, where $\sigma \simeq m_\pi^2/(4f_\pi^4) \simeq$ 25 mb. We also checked that this deceptively simple approximation is only accurate when the complexity of next-to-leading-order ChPT and the meson resonances are included. The second relaxation time, τ_f, was found to be of the order of 10 fm and is also roughly described by a similar formula. We argued that these long relaxation times are natural for a gas of pseudo-Goldstone bosons.

A computation in a pure meson gas cannot be used directly to understand chemical equilibration in heavy-ion collisions, because of the neglect of baryons. Nevertheless, it is interesting to compare these timescales with those of the fireball expansion rate near the crossover. The fireball probably cools through the crossover temperature at time between 1 and 10 fm [20]. While such a hydrodynamic computation is simplistic, it is in rough accord with the freeze-out time estimates of Ref. [8]. This timescale is much shorter than the slow mode relaxation time, indicating that our estimates of relaxation times, if applied to heavy-ion collisions, would be consistent with such estimates of the freeze-out time. Such an application would be especially interesting since it would directly utilize the hadronic cross sections which arise from chiral symmetry breaking to explain why chemical freeze-out would occur close to the chiral crossover in QCD, assuming that relaxation times in the high temperature phase are of the order of a femtometer. Since a dynamical origin for the numerical coincidence between $T_{\rm co}$ and $T_{\rm fo}$ would establish a deeper understanding of the strong interactions, this is certainly a direction worth exploring.

This speculation rests on the assumption that baryons would not change the relaxation time by orders of magnitude. Our justification for this is that one could extend the argument of eq. (13) to include the effect of adding baryons by writing a modified slow-mode relaxation time

$$\frac{1}{\tau_s'} \approx n_\pi^{eq}\sigma_{\pi\pi} + n_p^{eq}\sigma_{\pi p}. \tag{14}$$

We know that at low energies $\sigma_{\pi p}/\sigma_{\pi\pi} \simeq 2$, whereas $n_p^{\rm eq}/n_\pi^{\rm eq}$ varies between 0.001 and 0.01 when T changes from 100 to 150 MeV. This would imply that the effect of adding protons is a few percent. This is certainly not negligible, but it would not change the argument. Whatever reliability one assigns to this argument, it makes it extremely interesting to perform an accurate computation of this more realistic system using an appropriate higher-order ChPT. Unfortunately, this lies outside the scope of this paper. We hope to report the results of such a study in the near future.

APPENDIX A: ANALYSIS OF THEORY UNCERTAINTIES

This Appendix contains a detailed analysis of theoretical uncertainties arising from the LECs, through the example of the $\pi\pi$ scattering amplitude in the $J = I = 1$ channel. Below, the threshold for $K\bar{K}$ production there is only one reaction channel, and at the threshold, a second reaction channel opens up. We can therefore understand the errors as well as the discontinuities at the threshold through this one scattering channel.

The ChPT amplitude for $\pi\pi \to \pi\pi$ scattering below the $K\bar{K}$ threshold in the $J = 1$ and $I = 1$ channel is given by

$$T(s) = \frac{s-4m_\pi^2}{96\pi f_\pi^2}\left[1 - 4\mu_\pi - \frac{\mu_K m_\pi^2}{m_K^2} + \frac{s-10m_\pi^2}{64\pi^2 f_\pi^2} + \frac{4}{f_\pi^2}\{(-2L_1 + L_2 - L_3)s + 2(2L_4 + L_5)m_\pi^2\}\right] + P(s), \tag{A1}$$

where μ_i are scales related to the renormalization point

$$\mu_i = \frac{M_i^2}{32\pi^2 f_0^2}\log\frac{M_i^2}{\mu^2}, \tag{A2}$$

μ is chosen to be m_ρ, and the L_i are LECs evaluated at the scale μ. Apart from the factor of $P(s)$, the amplitude is a smooth, monotonically increasing polynomial in s and has no peaks. The function $P(s)$ has no closed-form expression, being defined in terms of the branch cuts due to intermediate kaon and eta states at one-loop order in ChPT. $T(s)$ increases

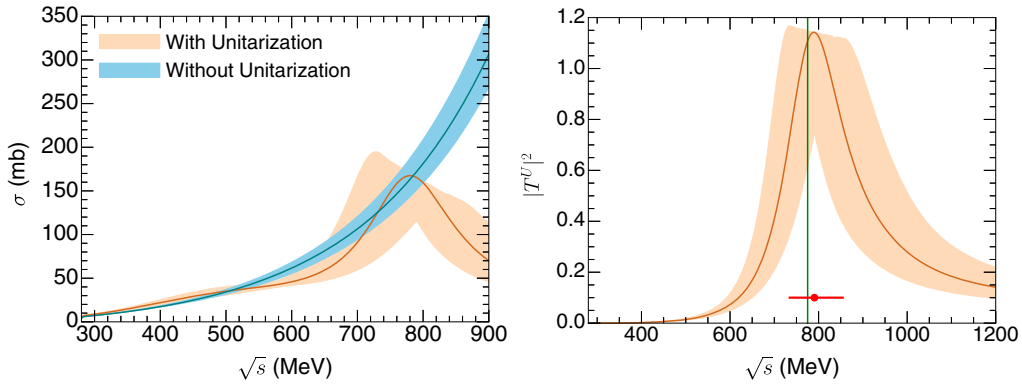

FIG. 4. The panel on the left shows the isospin-averaged $\pi\pi \to \pi\pi$ cross section obtained in the single-channel approximation with and without unitarization. Without unitarizing, the cross section increases without bound with increasing $\sqrt{s}$. Unitarization gives a sensible limit and obviates the need for an unphysical UV cutoff. The bands show the hypercube error estimates. The panel on the right shows the square of the unitarized single-channel amplitude for $I = J = 1$ (line and band for the central value and hypercube error estimates). The vertical line is the experimental value of the ρ meson mass, and the dot with the horizontal error bar shows the location of the peak in the amplitude with its spread from the hypercube error estimate.

smoothly with s and violates unitarity (as one sees from the increase in σ in Fig. 4). One can unitarize this, using the inverse amplitude method [21–23], and the resulting unitarized amplitude is

$$T^U(s) = \frac{s-4m_\pi^2}{96\pi f_\pi^2}\left[1 + 4\mu_\pi + \frac{\mu_K m_\pi^2}{m_K^2} - \frac{s-10m_\pi^2}{64\pi^2 f_\pi^2} - \frac{4(L_a s + 2L_b m_\pi^2)}{f_\pi^2} - \frac{96\pi f_\pi^2}{s-4m_\pi^2}P(s)\right]^{-1}, \tag{A3}$$

where we introduced the shorthand notation $L_a = -2L_1 + L_2 - L_3$ and $L_b = 2L_4 + L_5$. T^U has a pole off the physical sheet in the complex s plane, which is at the right position to provide a good description of the ρ resonance, as can be seen in Fig. 4. The single-channel problem shows very transparently how unitarization gives poles in the scattering amplitude. This NLO ampliutude contains only terms with J up to 1. It is possible that as higher-order terms in the T-matrix are computed the unitarized amplitude also contains poles corresponding to resonance with higher values of J. This is one motivation for a deeper study of ChPT beyond NLO.

The expression for the unitarized amplitude in eq. (A3) also shows that the amplitude depends only on two linear combinations of the parameters. Since L_a appears with the coefficient $4s/f_\pi^2$ and L_b appears with the coefficient $8m_\pi^2/f_\pi^2$, the amplitude is more sensitive to the combination L_a. Since reported values of the LECs give individual errors but no covariances, we compared two methods of evaluating the errors on the combinations L_a and L_b.

In this explanation of the methods, we use the notation $\bar{L}_i$ for the reported central value and δL_i for the reported error. It is useful to consider deviations from the mean in units of the error; i.e., we can write for an arbitrary value $L_i = \bar{L}_i + \delta L_i x_i$. The Gaussian method consists of sampling values of x_i independently from a Gaussian distribution of unit width around zero. Contours of equal probability are hyperspheres centered on the origin in the space of $\{x_i\}$. Any linear combination can be sampled through this method and the errors established through the usual statistical methods. The sampling by a Gaussian ignores all covariances between the errors in the LECs.

The alternative method erects a unit hypercube in the space of $\{x_i\}$ and samples the error bounds on L_a and L_b in this volume. Opposite "faces" of the hypercube correspond to errors $\pm\delta L_i$ on the sample. The corners of the hypercubes are points where all the errors conspire to add or to cancel each other maximally. Sampling the values at the corners gives the maximum possible covariances between the errors. If the LECs appeared linearly in the amplitude, then the corners would be extrema in the amplitudes. This would be true for the ununitarized amplitude in eq. (A1). However, after unitarization, the amplitude in eq. (A3) is no longer linear in the LECs, so the corners extremize the errors only if the mathematical extremum lies outside the hypercube (this happens for T^U). The corners are still points where the errors in the LECs conspire to cancel or add up maximally.

For the case of T^U, the comparison of error bounds from the two methods is fairly straightforward. Since two linear combinations of five LECs are involved, we need to consider the projections of the unit hypercube and unit hypersphere in five dimensions to a two-dimensional plane. The unit hypersphere projects to a unit circle. For the particular plane corresponding to the linear combinations

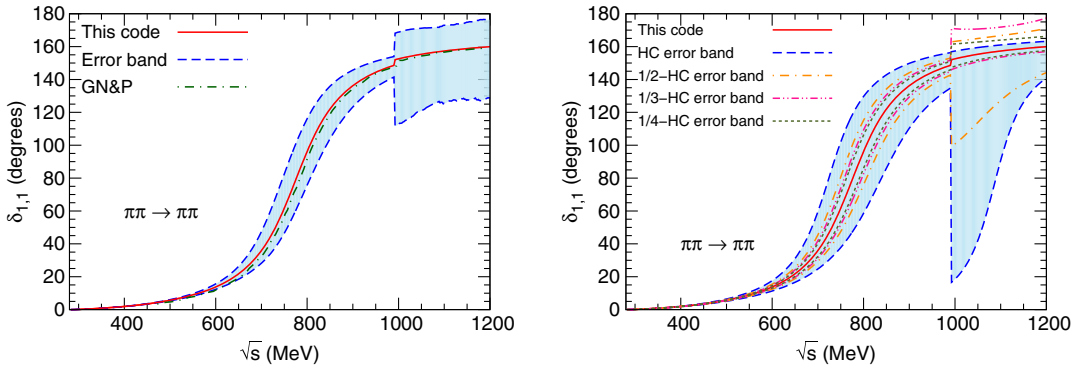

FIG. 5. The scattering phase shift $\delta_{1,1}$ and its uncertainties, shown as a function of $\sqrt{s}$ (using the Gaussian method in the left panel and the hypercube on the right). The thick full line shows the result when using $\bar{L}_i$ and the shaded band bounded by dashed lines the error estimates. In the panel on the right, we also show the errors when the size of the hypercube is changed.

L_a and L_b, the hypercube projects to a rectangle with sides between ± 4 in the (scaled) L_a direction and ± 3 in the (scaled) L_b direction. So, in this case, the hypercube errors are definitely larger, because they examine only the special cases with maximum covariance between errors.

Above the $K\bar{K}$ threshold T is a 2×2 matrix. We choose the 11 component to be the amplitude of the $\pi\pi \to \pi\pi$ channel. It turns out that apart from the combinations L_a and L_b the matrix also depends on the combination $L_c = 4L_1 - 2L_2 + L_3$, as well as L_3, L_4, and L_5 separately. As a result, one can decompose this into the independent combination $L' = 2L_1 - L_2$ and the other three LECs. Unitarization mixes the components of the matrix so that the 1,1 component of the unitarized matrix is some combinations of the different amplitudes. As a result, just below the threshold, the uncertainties come from two linear combinations of five of the LECs. Just above, they come from four different combinations of the same five. This is the main reason for the discontinuity in the width of the error band at the threshold, as shown in Fig. 5.

The special covariances sampled by the hypercube have a large effect in this case, as one sees. The first thing to notice is the huge excursion allowed in the lower limit of the errors. To understand this further, we do the following analysis immediately above the threshold. Join the center of the hypercube with the corner, which gives the minimum of the uncertainty band. As we proceed along this line, we find that the phase of the amplitude changes continuously. At the center, the phase is in the second quadrant (between $\pi/2$ and π) and remains in this range, while decreasing, until about 85% of the distance to the corner is covered. After that, it crosses over to the first quadrant (phase angle between 0 and $\pi/2$). This is clearly seen in the second panel of Fig. 5, in which we report the errors when the unit hypercube is changed to one with sides of size 1/2, 1/3, and 1/4. The lower error band shrinks very rapidly.

The other interesting effect is that the upper limit of the errors is larger when the Gaussian method is used. One can understand this by noting that 1/3 hypercube gives the largest upper bound on the error. This happens because the error in $\delta_{1,1}$ is not linear in the δL_i, and the extremum lies inside the hypercube. The Gaussian error determination does not suffer from either pathology. This is why we adopt the Gaussian method in this paper.

APPENDIX B: CONSERVED QUANTITIES IN THE MESON GAS

The net strangeness is a conserved quantity in strong interaction processes. Furthermore, when the temperature is low enough that $2 \to 2$ reactions are dominant, the total number of particles is conserved. The net electrical charge is also conserved, and if we were to distinguish between the different charges of the pions, we would have to keep that in mind, too. However, since we neglect that difference, charge conservation, i.e., isospin conservation, may be neglected. A microcanonical ensemble of the meson gas then needs three different extensive quantities: the energy (E), the total particle number (N), and the total strangeness (S). The grand canonical ensemble is, correspondingly, described by three thermodynamic intensive parameters, namely, the temperature T and the chemical potentials μ_N and μ_S corresponding to the two conserved numbers. In terms of the entropy, Σ, one may define these as usual,

$$T = \left.\frac{\partial E}{\partial \Sigma}\right|_{N,S} \qquad \mu_N = \left.\frac{\partial E}{\partial N}\right|_{\Sigma,S} \qquad \mu_S = \left.\frac{\partial E}{\partial S}\right|_{\Sigma,N}. \tag{B1}$$

In the heavy-ion physics literature [6–8], it is more common to introduce a chemical potential for each hadron in the phase below the crossover. In our case, the particles are π, K, $\bar{K}$, and η. Their numbers are related to the conserved quantities by $n_\pi + n_K + n_{\bar{K}} + n_\eta = N$, and $n_{\bar{K}} - n_K = S$. Then, using the chain rule, one can evaluate

$$\mu_\pi = \left.\frac{\partial E}{\partial n_\pi}\right|_{\Sigma,n_K,n_{\bar{K}},n_\eta} = \mu_N \quad \mu_K = \left.\frac{\partial E}{\partial n_K}\right|_{\Sigma,n_\pi,n_{\bar{K}},n_\eta} = \mu_N - \mu_S$$
$$\mu_\eta = \left.\frac{\partial E}{\partial n_\eta}\right|_{\Sigma,n_\pi,n_K,n_{\bar{K}}} = \mu_N$$
$$\mu_{\bar{K}} = \left.\frac{\partial E}{\partial n_{\bar{K}}}\right|_{\Sigma,n_\pi,n_K,n_\eta} = \mu_N + \mu_S. \tag{B2}$$

The observed net yields in heavy-ion collisions have been fitted to thermal gas models with small values of μ_S and with nearly vanishing isospin chemical potential [1,2]. The Goldstone boson densities which come out of these corresponds to using $\mu_N \simeq \mu_S \simeq 0$. On the other hand, Ref. [8] has explored μ_π as large as 60 MeV. We report our main results for $\mu_N = \mu_S = 0$ but also show estimates of the relaxation time when μ_N is as large as 100 MeV.

[1] A. Andronic, P. Braun-Munzinger, K. Redlich, and J. Stachel, Nature (London) **561**, 321 (2018).
[2] J. Cleymans, M. Marais, and E. Suhonen, Phys. Rev. C **56**, 2747 (1997); A. Majumder and V. Koch, Phys. Rev. C **68**, 044903 (2003); V. Begun, L. Ferroni, M. I. Gorenstein, M. Gazdzicki, and F. Becattini, J. Phys. G **32**, 1003 (2006); T. Csorgo, R. Vertesi, and J. Sziklai, Phys. Rev. Lett. **105**, 182301 (2010); J. Cleymans and D. Worku, Mod. Phys. Lett. A **26**, 1197 (2011); R. Singh, L. Kumar, P. K. Netrakanti, and B. Mohanty, Adv. High Energy Phys. **2013**, 761474 (2013); S. Chatterjee, R. Godbole, and S. Gupta, Phys. Lett. B **727**, 554 (2013); V. Begun, W. Florkowski, and M. Rybczynski, Phys. Rev. C **90**, 054912 (2014); D. Oliinychenko, K. Bugaev, V. Sagun, A. Ivanytskyi, I. Yakimenko, E. Nikonov, A. Taranenko, and G. Zinovjev, arXiv:1611.07349; V. Vovchenko, M. I. Gorenstein, and H. Stoecker, Phys. Rev. C **98**, 064909 (2018); J. Cleymans, B. Hippolyte, M. W. Paradza, and N. Sharma, Int. J. Mod. Phys. E **28**, 1940002 (2019); S. Gupta, D. Mallick, D. K. Mishra, B. Mohanty, and N. Xu, arXiv:2004.04681; S. Bhattacharyya, D. Biswas, S. K. Ghosh, R. Ray, and P. Singha, Phys. Rev. D **101**, 054002 (2020).
[3] Y. Aoki, S. Borsanyi, S. Durr, Z. Fodor, S. D. Katz, S. Krieg, and K. K. Szabo, J. High Energy Phys. 06 (2009) 088.
[4] A. Bazavov *et al.* (HotQCD Collaboration), Phys. Lett. B **795**, 15 (2019).
[5] H. Bebie, P. Gerber, J. L. Goity, and H. Leutwyler, Nucl. Phys. **B378**, 95 (1992).
[6] J. L. Goity, Phys. Lett. B **319**, 401 (1993).
[7] M. Prakash, M. Prakash, R. Venugopalan, and G. Welke, Phys. Rep. **227**, 321 (1993).
[8] C. M. Hung and E. V. Shuryak, Phys. Rev. C **57**, 1891 (1998).
[9] D. Fernandez-Fraile and A. G. Nicola, Phys. Rev. D **80**, 056003 (2009).
[10] M. Bleicher *et al.*, J. Phys. G **25**, 1859 (1999); H. Petersen, M. Bleicher, S. A. Bass, and H. Stocker, arXiv:0805.0567.
[11] Z. W. Lin, C. M. Ko, B. A. Li, B. Zhang, and S. Pal, Phys. Rev. C **72**, 064901 (2005); Z. W. Lin, Indian J. Phys. **85**, 837 (2011).
[12] J. Goldstone, A. Salam, and S. Weinberg, Phys. Rev. **127**, 965 (1962).
[13] S. Weinberg, Physica (Amsterdam) **96A**, 327 (1979).
[14] J. Gasser and H. Leutwyler, Ann. Phys. (N.Y.) **158**, 142 (1984).
[15] G. Amoros, J. Bijnens, and P. Talavera, Nucl. Phys. **B585**, 293 (2000).
[16] A. G. Nicola and J. R. Pelaez, Phys. Rev. D **65**, 054009 (2002).
[17] E. W. Kolb and M. S. Turner, Front. Phys. **69**, 1 (1990).
[18] M. Cannoni, Int. J. Mod. Phys. A **32**, 1730002 (2017).
[19] M. Tanabashi *et al.* (Particle Data Group), Phys. Rev. D **98**, 030001 (2018).
[20] P. Bozek and I. Wyskiel, Phys. Rev. C **79**, 044916 (2009).
[21] T. N. Truong, Phys. Rev. Lett. **61**, 2526 (1988).
[22] A. Dobado, M. J. Herrero, and T. N. Truong, Phys. Lett. B **235**, 129 (1990).
[23] T. Hannah, Phys. Rev. D **55**, 5613 (1997).